The average streamline plot bears strong similarity to the measurements.[1] The measured locations of the forward and aft-stagnation points are 1.2 and $0.8D_a$. The difference between the experimental results and the numerical results is due to the small difference in the velocity ratio between the computed and experimental flows (as well as other secondary effects corresponding to the density difference between the two streams in the experiment). Quantitative comparisons between the computed and measured mean velocity profiles at different sections show good agreement, remarkably without resorting to any adjustable parameters.[6]

The effect of the velocity ratio on the flow structure is summarized in Fig. 5 where we show the locations of the forward and aft-stagnation points in terms of the velocity ratio up to $V_j = 0.667$. The two curves are extrapolated until they intersect at $V_j = 0.68$, at which the two stagnation points overlap and the structure of the recirculation zone changes. Beyond this critical velocity ratio, the stagnation point moves away from the axis and the inner jet penetrates through the recirculation zone.[5,7] This regime has been called the inner jet-dominated flow, in contrast to the annular flow-dominated regime at lower jet velocities, and the transition regime.

Figure 5 shows the difference between the two regimes discussed here, the annular flow-dominated regime and the transition regime. In the first regime, for $V_j < V_{trans}$, the forward-stagnation point moves forward and the aft-stagnation point moves backward very slowly with increasing jet velocity. The value of V_{trans} is difficult to determine precisely; the figure indicates that $V_{trans} > 0.5$. For higher jet velocity, both stagnation points move towards each other very rapidly as the jet velocity increases, the flow is highly unsteady in the wake region and is very sensitive to the jet velocity. Since this unsteadiness is not due to an unsteady boundary condition, it is generated by an instability that amplifies small perturbations randomly introduced in the flow. Contrary to the annular flow regime where the jet is stagnated close to the bluff-body, the fast penetration of the jet into the recirculation zone during transition is accomplished by the destabilization of the recirculation zone and the formation of large scale structures.

Comparison with $V_j = 1.0$

In the case of $V_j = 1.0$, the flow is strongly unsteady, and the dominant frequency of oscillation on the outside diameter of the bluffbody is $f = 0.135$. This is very close to the dominant frequency in the current case. On the other hand, the second subharmonic is at $f = 0.05$. In this case, we noticed a quiet period after two composite structure sheddings. There is an indication that the flow looses some of its organization as the jet velocity increases and that this quiet period between shedding becomes longer.[6]

Acknowledgments

The work is partially funded by the Gas Research Institute program with Altex Technologies, Inc., the Air Force Office of Scientific Research Grant 840356, the National Science Foundation Grant CBT-8709465, and the Department of Energy Grant DE-FG04-87AL33875. Some of the computations were performed using grants from the John von Neumann National Supercomputer Center and the Illinois National Supercomputer center.

References

[1]Kelly, J. T., Namazian, M., Schefer, R. W., and Perrin, M., "Characterization of Non-Premixed Bluff-Body Burner Flames," 1990 GRI Annual Rept., GRI89/0150, 1989.

[2]Roquemore, W. M., Britton, R. L., and Sandhu, S. S., "Investigation of the Dynamic Behavior of a Bluff-Body Duffusion Flame Using Flame Emission," AIAA Paper 82-0178, Jan. 1982.

[3]Kenworthy, J. S., "The Flow and Mixing in Double Concentric Jets," Ph.D. Thesis, Univ. of Sheffield, Sept. 1971.

[4]Li, X., and Tankin, R. S., "A Study of Cold and Combusting Flow Around Bluff-Body Combustor," Spring Meeting of the Western States Section, The Combustion Institute, NASA Lewis Research Center, Cleveland, OH, May 5-6, 1986.

[5]Martins, L.-F., and Ghoniem, A. F., "Simulation of the Nonreacting Flow in a Bluff-Body Burner," ASME Winter Annual Meeting, Dallas, TX , Nov. 26-30, 1990.

[6]Martins, L.-F., "Vortex Computations of Axisymmetric High Reynolds Number Flows in Complex Domains," Ph.D. Thesis, Dept. of Mechanical Engineering, Massachussetts Inst. of Technology, Cambridge, MA, June 1990.

[7]Martins, L.-F., and Ghoniem, A. F., "Vortex Simulation of Bluff-Body Flow Dynamics; Jet Penetration at High Velocity Ratios," AIAA/ASME/SAE/ASEE 27th Joint Propulsion Conf., Sacramento, CA, July 24-27, 1991.

[8]Michalke, A., and Hermann, G., "On the Inviscid Instability of a Circular Jet with External Flow," *Journal of Fluid Mechanics*, Vol. 111, 1982, pp. 343-359.

Viscous Eddies over a Grooved Surface Computed by a Gaussian-Integration Galerkin Boundary-Element Method

P. Luchini,* F. Manzo,† and A. Pozzi‡
University of Naples, Naples 80125, Italy

Introduction

IT is a well-known fact that low-Reynolds-number flows (solutions of the Stokes equations) may exhibit recirculation structures (viscous eddies) in the proximity of corners.[1] These have been observed in various geometries, for instance in Ref. 2, and were also recently found to occur in flow over a grooved surface through an analogical simulation realized by bending a suitably constrained elastic thin plate.[3]

The interest in flows over grooved surfaces has been raised in recent years by the attempts to use such surfaces for drag reduction in a turbulent stream. Several authors (see, e.g., Refs. 3, 4, and references therein) have experimentally found that a drag reduction can indeed be achieved. Bechert and his collaborators[4] proposed a qualitative mechanism of the phenomenon, in which a dominant role is played by the viscous sublayer of the turbulent stream, and calculated the effect upon the mean flow of longitudinal grooves (or riblets, depending on the way one wishes to see them) of a height comparable to the thickness of the viscous sublayer. Within the approximation given by the Stokes equations, the effect of the grooved wall is characterized by the presence of an effective plane wall that the velocity profile appears to originate from. The distance of this effective plane wall from the riblet tips takes the name of longitudinal protrusion height.

The basic action that riblets are assumed to exert is a damping of the crossflow vortices that accompany the turbulent flow. In this way they effect a reduction of the near-wall level of turbulence, and thus of the eddy viscosity and ultimately of the drag. In Ref. 5 the present authors, analytically in some geometries and numerically in others, calculated the transverse flow across the grooves within the same approximation (Stokes equations) that had been adopted in Ref. 4 for the longitudinal motion, determining the value of the transverse protrusion height and therefore of the protrusion-height dif-

Received July 31, 1991; revision received Dec. 15, 1991; accepted for publication Dec. 20, 1991.

*Staff Research Scientist, Istituto di Gasdinamica, Facoltà di Ingegneria, P.le Tecchio 80.

†Associate Professor, Istituto di Gasdinamica, Facoltà di Ingegneria, P.le Tecchio 80.

‡Professor, Istituto di Gasdinamica, Facoltà di Ingegneria, P.le Tecchio 80.

ference, which measures the differential action of the grooves on longitudinal flow and crossflow.

In Ref. 5 the protrusion heights only were discussed. In fact, the numerical algorithm, being of the boundary-element type, can obtain the boundary values of the relevant physical quantities, and hence the protrusion heights, without ever considering values at internal points of the computational domain. Internal values can, nevertheless, be recovered from the boundary-element solution if one wished to. In this Note, we want to present some typical streamline patterns that arise in Stokes flow across riblets, exhibiting viscous eddies.

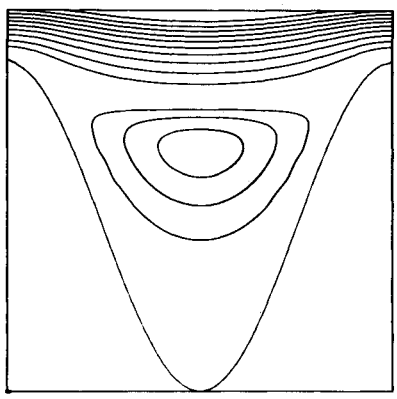

Fig. 1 Stokes flow along a cosinusoidal wall, with a maximum height of the cosinusoidal profile equal to the period. Streamlines are drawn for positive values of ψ increasing at constant step 0.1 from $\psi = 0.1$ (overrunning flow) and negative values of ψ decreasing at constant step -0.02 from $\psi = -0.02$ (bound vortex). At the wall $\psi = 0$.

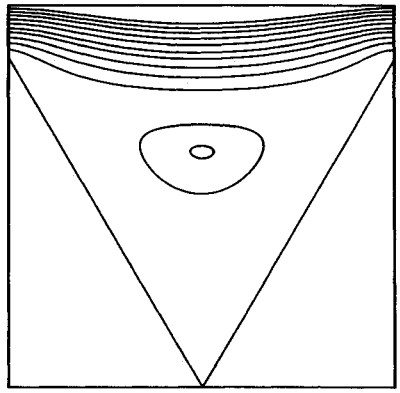

Fig. 2 Stokes flow across triangular grooves, with a maximum height equal to the period. Streamlines drawn for the same values of ψ as in Fig. 1.

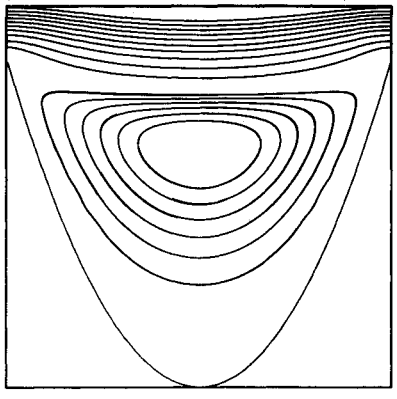

Fig. 3 Stokes flow across parabolic grooves, with a maximum height equal to the period. Streamlines drawn for the same values of ψ as in Fig. 1.

Gaussian-Integration Galerkin Numerical Algorithm

For the present work, we needed boundary-element algorithms that would determine solutions of both the Laplace and the biharmonic equation near a periodic corrugated wall. For the Laplace equation, we enforced periodicity directly by choosing a periodic Green function. With this choice the boundary integral that represents the harmonic function $f(x,y)$ may be extended to a single period of the boundary only, and thus written as

$$f(x',y') = \int_0^{2\pi} \left\{ f[x,y_0(x)] \frac{\partial G}{\partial n} \frac{ds}{dx} - G(x-x', y-y')\phi(x) \right\} dx \tag{1}$$

where $\phi(x) = \partial f/\partial n\ [x,y_0(x)]\ ds/dx$ and the Green function $G(x-x',y-y') = (4\pi)^{-1}\{\log[2\cosh(y-y') - 2\cos(x-x')] - y + y'\}$.

According to the general boundary-element philosophy, we particularize Eq. (1) to $y' \to y_0(x')$ (with some care needed in taking the limit from the interior) and interpret the result as an integral equation relating the two functions $f[x,y_0(x)]$ and $\phi(x)$, either one of which may be the unknown.

Once the integral equation is formulated, in order to be solved numerically it must be discretized, which means both that the unknown function must somehow be represented in terms of a finite number of unknown parameters and that the integral equation over a continuous domain must be replaced by a finite number of algebraic equations. For this purpose, we have developed a hybrid technique that tries to combine the advantages of the Galerkin method with the simplicity of collocation.

The two main ingredients of this technique are the representation of f and ϕ through piecewise polynomials and the adoption of a Gaussian integration formula for all of the required integrals. Let the interval $(0,2\pi)$ be divided up into N, generally disuniform, subintervals (x_i,x_{i+1}). In each subinterval, we assume every unknown, say ϕ, to be represented by a polynomial of order $(M-1)$, and approximate the integral of this polynomial times the Green function by an M-point Gaussian formula, i.e., by the sum of the values taken by the integrand at M purposely chosen points, multiplied by suitable weights. The key property of Gaussian integration, which is also exploited in other numerical techniques such as the spectral-element method for partial differential equations, is that it is exact for polynomials up to order $(2M-1)$, so that we are effectively approximating the Green function through a polynomial of order M in each subinterval. At the same time, we do not need to deal with the polynomial representation of ϕ explicitly, because we can simply adopt as variables the values of ϕ at the M Gaussian integration points in each subinterval, and never let the M coefficients of the polynomial appear at all.

The reduction of the integral equation to a finite system is executed in the Galerkin manner, that is by first multiplying the equation itself by a test function $T(x')$ and integrating over $(0,2\pi)$, and then discretizing this new integral in the same way as the preceding one. Again, no integral need actually be computed, either analytically or numerically, because requiring the equation to be satisfied for T being any piecewise polynomial of order $(M-1)$ over the chosen partition into N intervals is equivalent to requiring that the equation be satisfied pointwise at the Gaussian integration points (zeroes of Legendre polynomials). We can thus implement the technique as though it were a collocation one, but obtain the advantages of a Galerkin formulation.

Results and Conclusions

In the application of the preceding technique to Eq. (1) there are some other complications, in that the kernel, either G or $\partial G/\partial n$, has a singularity at $x = x'$, and in that the integral

equation itself is singular, in the sense that it admits a nonzero solution with a zero known term and conversely is not guaranteed to have finite solutions unless the known term satisfies a condition. The reader is referred to Ref. 5 for these additional details, which have no bearing on the basic Gaussian-integration Galerkin technique; suffice it to say here that the condition needed to remove the singularity of the integral equation is the very one that allows the velocity gradient at infinity to be specified among the boundary conditions.

Once a general solving procedure for the Laplace equation is available, the biharmonic equation of Stokes flow is solved by first reformulating the problem as two Laplace equations with coupled boundary conditions and then discretizing the boundary integrals that represent these two equations in the manner just described. It is, in fact, well known (and very easily verified) that a general solution of the biharmonic equation may be written as $\psi = f + yg$, where $f(x,y)$ and $g(x,y)$ are harmonic functions. The solution of the biharmonic equation thus involves the inversion of only one $MN \times MN$ matrix, in addition to the one already inverted in solving the Laplace equation, rather than the much slower inversion of a $2MN \times 2MN$ matrix which would be entailed by a direct boundary-element formulation of the biharmonic equation in terms of its own Green function.

After the boundary problem has been solved, internal values of the stream function may be calculated, as $\psi = f + yg$, by applying the general formula (1) to f and g separately. The necessary integrals are once more evaluated by Gaussian integration. The results thus obtained are plotted in Figs. 1–3, respectively, for a cosinusoidal, triangular, and parabolic groove profile. All of the computations were done with first-order interpolating polynomials, using 30 uniform subintervals for Figs. 1 and 3 and 70 uniform subintervals for Fig. 2, and are precise to within graphical accuracy.

It may be noticed that the bound vortex is strongest in the parabolic case and weakest in the triangular case, as might intuitively have been expected on the basis of wall conformation. In all three cases there is almost certainly a second vortex below the one plotted, but its intensity is too weak and falls below the threshold of computational errors. In the triangular case there must be an infinite hierarchy of vortices as well, according to the general results of Ref. 1, but of course successive members of this hierarchy are even weaker.

References

[1]Moffat, H. K., "Viscous and Resistive Eddies Near a Sharp Corner, *Journal of Fluid Mechanics*, Vol. 18, Pt. 1, Jan. 1964, pp. 1–18.

[2]Taneda, S., "Visualization of Separating Stokes Flows," *Journal of the Physical Society of Japan*, Vol. 46, No. 6, 1979, pp. 1935–1942.

[3]Bechert, D. W., Bartenwerfer, M., and Hoppe, G., "Turbulent-Drag Reduction by Nonplanar Surfaces — A Survey of the Research at TU/DLR Berlin," *Proceedings of the IUTAM Symposium on Structure of Turbulence and Drag Reduction*, edited by A. Gyr, Springer, Berlin, 1990, pp. 525–543.

[4]Bechert, D. W., and Bartenwerfer, M., "The Viscous Flow on Surfaces with Longitudinal Ribs," *Journal of Fluid Mechanics*, Vol. 206, Sept. 1989, pp. 105–129.

[5]Luchini, P., Manzo, F., and Pozzi, A., "Resistance of a Grooved Surface to Parallel Flow and Cross-Flow," *Journal of Fluid Mechanics*, Vol. 228, July 1991, pp. 87–109.